POLITECNICO DI TORINO
Repository ISTITUZIONALE

Retrofitting of an Industrial DLN Gas Turbine Combustor for Fuel-Flexible Hydrogen Applications

Original
Retrofitting of an Industrial DLN Gas Turbine Combustor for Fuel-Flexible Hydrogen Applications / Carusotto, S., Capalbo, N., Salvadori, S., Cavalli, A., Cardile, F., Misul, D.A.. - ELETTRONICO. - 663:(2025), pp. 1-11. (International Gas Turbine Conference 2025 (IGTC 2025) Brussels, Belgium October 14-15, 2025) [10.1051/e3sconf/202566301005].

Availability:
This version is available at: 11583/3004356 since: 2026-01-15T18:17:51Z

Publisher:
E3S Web of Conferences

Published
DOI:10.1051/e3sconf/202566301005

Terms of use:

This article is made available under terms and conditions as specified in the corresponding bibliographic description in the repository

Publisher copyright

(Article begins on next page)

14 September 2026

Retrofitting of an Industrial DLN Gas Turbine Combustor for Fuel-Flexible Hydrogen Applications

Salvatore Carusotto[1], *Niccolò* Capalbo[1], *Simone* Salvadori[1], *Alberto* Cavalli[2], *Francesco* Cardile[2], *Daniela Anna* Misul[1]

1 Department of Energy, Politecnico di Torino, Turin, Italy
2 EthosEnergy Italia S.p.a., Turin, Italy

Abstract. The use of lean-premixed combustion systems in gas turbines for power generation represents one of the most effective options to achieve low NO_x emissions under dry conditions. Modern swirl burners can guarantee very low emissions and stable operation when traditional fuels (i.e., methane or natural gas) are used. However, these systems could be affected by flashback and could generate an increase in NO_x emissions when they are fed with hydrogen blends. Considering the complexity of these systems and the fact that they are operated close to harmful conditions, it is necessary to schedule a periodic maintenance of the combustor and replacement of the injection system, implying maintenance costs, power plant shutdown, and environmental impact. This work follows a series of already performed studies on the injection system and the combustion chamber for a 5 MW machine. Both the available dataset obtained from reactive numerical simulations and the observations in the grade of deterioration registered during the maintenance phase are used as retrofitting guidelines for the definition of an innovative design of the injector/combustor geometries. The newly designed configuration is numerically tested both at natural gas conditions and in the case of hydrogen blends, thus guaranteeing both stability at different fuel compositions and the extension of the service intervals for the upgraded design.

1 Introduction

The adoption of lean-premixed combustion systems in gas turbines can be dated back to the early 1990s, driven by growing concerns over pollutant emissions, in particular regarding nitrogen oxides (NO_x). Dry-Low-NO_x (DLN) combustors are designed to mix fuel and air within the injection system before entering the combustion chamber, thus operating near the lean flammability limit. This approach reduces the flame temperature, which is key to limiting thermal NO_x emissions, as their formation increases exponentially with temperature [1]. Today's regulatory goals focus not only on cutting NO_x emissions — a priority in climate change mitigation — but also on achieving carbon neutrality by 2050 [2]. This pushes gas turbine manufacturers to explore alternative systems capable of handling alternative fuel types such as hydrogen or ammonia [3]. While the adoption of green hydrogen holds promise for balancing renewable energy fluctuations when used in gas turbine power plants, it poses significant flashback risks [4]. Modern swirl burners perform well with conventional fuels, ensuring stable combustion and low emissions, but hydrogen blending is generally limited at around 60% by volume to avoid flashback [5]. The current state of the art for gas turbine combustors consists of several concepts designed for higher hydrogen content, with various approaches among manufacturers [6], as in the Ansaldo GT36, which exploits sequential combustion [7]. Another option involves jet burner configurations, as in the POShyDON burner of TU Berlin [8] or in the combustion concepts of DLR for Gas Turbines (GTs) [9] and Micro Gas Turbines (MGTs) [10]. However, such technologies are still rare in large-scale industrial use and mostly still operated at ambient pressure conditions. Even though these solutions will be increasingly important, two practical industrial considerations must be kept in mind. First, lifetime extensions will be needed for existing power plants to avoid considerable costs for new installations. Second, green hydrogen production costs are expected to remain high in the near future, making it unlikely that large amounts of hydrogen will be blended into carbon-based fuel mixtures. Low-percentage hydrogen blending in natural gas networks is a more probable scenario [6]. Retrofitting existing plants for hydrogen use is already well-established, especially with diffusive combustors, known for their high stability, as studied by the authors in [11][12]. However, using hydrogen leads to higher temperature distributions due to its higher lower heating value (LHV), around 120 MJ/kg. In diffusive flames, combustion occurs at stoichiometric conditions, so flame temperature is directly linked to LHV. This requires NO_x reduction measures such as water or steam injection [13], which can lower overall plant efficiency. Within this framework, this paper shows a possible redesign strategy, validated numerically, for an existing annular gas turbine combustor equipped with a DLN injection system, aiming at guaranteeing fuel flexibility for hydrogen-enriched natural gas blends up to 50% vol content. The main goal is to obtain a modular design which shows stable operability and constant NO_x emissions levels when switching from natural gas to hydrogen-enriched blends while also limiting the thermal stresses on the injector components. This work follows a series of studies already performed on the same machine. The injection system was already

© The Authors, published by EDP Sciences. This is an open access article distributed under the terms of the Creative Commons Attribution License 4.0 (https://creativecommons.org/licenses/by/4.0/).

investigated by the authors in terms of mixing performance for natural gas conditions in a previous publication [14]. Subsequently, the assessment of the effects of hydrogen addition has been performed by using a series of reactive 3D-CFD RANS simulations performed with an approach aiming at maintaining the computational costs at a reasonable level [15]. Therefore, the injector was no longer included in the fluid domain while it was coupled with a procedure that will be shown in section 3.1.

This paper starts by introducing the main features of the investigated machine in Section 2. The adopted numerical setup is the same as discussed in [15] and used again for the assessment of the redesigned version in this study (Section 3). The hydrogen addition effects are recalled in Section 4 and used to evaluate the redesign requirements. In Sections 5 and 6, the redesign strategy and results are finally discussed.

2 Description of the test case

The combustor under investigation features an annular geometry and is mounted on a gas turbine that produces approximately 5 MW of net power at base load. Originally designed for natural gas, this combustor is being evaluated for operation with blends containing up to 50% hydrogen by volume, a range consistent with the contemporary research context discussed in the introduction. During the investigation, the thermal power is held constant by ensuring the product of the fuel mass flow rate and lower heating value (LHV) remains unchanged regardless of blend composition - a standard approach for comparing different fuels under equivalent energy input conditions. As blends incorporate more hydrogen, the fuel composition is adjusted.

The simulated fluid domain, shown in Figure 1, consists of a 30° sector of the combustor, which includes part of the annular chamber and the end section of the injector. Including only the final portion of the injector (marked in cyan in Figure 1) ensures proper coupling between the combustion chamber and injector while minimising the number of grid elements.

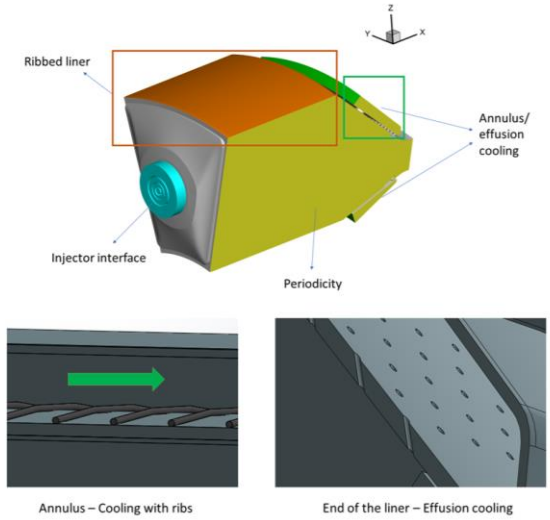

Figure 1: Isometric view of the combustion chamber - detailed view of the cooling systems for the liner.

This approach, based on the previous study [14], helps simplify the model without sacrificing the consistency and accuracy of the results. The compressed air flows through the annulus to cool the liner before it passes into the dilution and cooling holes. Tubular ribs are placed along the liner's outer surface to enhance this cooling effect by increasing the turbulence level.

Additionally, the liner's end and the dome are cooled by using effusion cooling techniques.

The simulated domain also includes the Transition Piece (TP), which serves as the connection between the combustor and the turbine. The injection system features 12 injectors, as detailed in previous research by the authors [14]. Only a 30° sector of the combustor is modelled in the simulation, taking advantage of the system's periodicity.

3 Numerical Method

The modelling approach adopted in this work is directly derived from previous research on evaluating the effects of hydrogen addition for the same combustor [15]; however, it is briefly reported here for completeness.

Numerical simulations of the DLN combustor were conducted using the commercial software ANSYS® FLUENT® 2022 R2 [15]. The turbulent behaviour inside the combustor was captured by solving the Reynolds-averaged Navier-Stokes (RANS) equations under steady-state conditions. For the pressure-velocity coupling, the SIMPLE scheme is applied, a widely used method suited for incompressible or mildly compressible flows. The spatial discretization of the flux terms in the governing equations is handled using a second-order upwind scheme for all variables.

The adopted mesh is unstructured and hybrid, with the use of prismatic elements in the wall regions and tetrahedra in the core regions. The grid shows three prismatic layers with resulting y+ values between 30 and 300 in accordance with the used turbulence model, the k-ε renormalisation group (RNG) [17]. The turbulence model is widely used in several combustion problems and has proved to be suitable for swirled stabilised flames [18]. The adopted grid comprises about 26 million elements, a relatively large number of elements for a RANS simulation. Such a number is justified by both the fluid domain dimensions and the detailed modelling of many components, i.e., the annulus, the cooling system, and the injector interface. To guarantee the lack of influence on spatial discretization, a grid sensitivity analysis is performed in a simplified domain, where the annulus and the cooling model are removed, thus leading to a base grid consisting of 14 million elements. The latter is hence compared to two other grids, namely a coarse and a fine one featuring 7 million and 31.5 million elements, respectively. Since no relevant differences were detected between the base and fine grid results, the element density associated with the base grid was selected for the study, thus validating the 26 million elements one.

Figure 2 presents a cross-section of the mesh applied in the final analysis, shown along a longitudinal

plane. The grid is noticeably more refined in the central region, where the flame is situated, as well as in the dilution zone, characterized by intense mixing. This enhanced resolution helps to minimize numerical diffusion. Additionally, a close-up of the area indicated by the yellow outline is provided to illustrate the local density of mesh elements. In this region, the typical size of the tetrahedral elements is approximately 1mm.

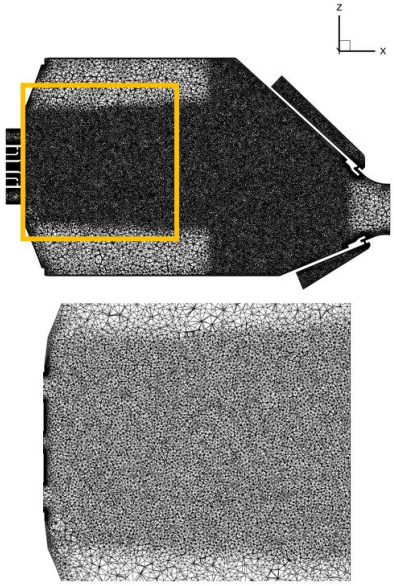

Figure 2: Mesh, front section view.

The combustion model employed in this study is the Flamelet Generated Manifold (FGM) model introduced by van Oijen and de Goey [19]. ANSYS® FLUENT® classifies this model as partially premixed due to its flexibility, allowing it to be applied to both premixed and diffusive flames. Given that the burner under investigation features both flame types - because of the pilot presence - the FGM model is a reasonable choice within the solver when using a tabulated approach. To faithfully represent the operating conditions of the combustor, the "Premixed Flames" option is selected, since 96% of the fuel is injected into the main circuit under technically premixed conditions. This approach relies on two variables (internal passive scalars): the mixture fraction (f) and the reaction progress variable (c), which parameterize the temperature and species mass fractions involved in combustion. Specifically, ANSYS® FLUENT® calculates the mean mixture fraction and mean reaction progress variable (non-normalized), along with their variances, throughout the fluid domain by solving four transport equations. These variables are then used as input for pre-tabulated look-up tables derived from prior 1D premixed flame computations. Turbulence-chemistry interaction is modeled using a Probability Density Function (PDF), assumed to have a beta distribution shape. More precisely, the PDF is the product of two beta PDFs and accounts for the fluctuations in both mixture fraction and reaction progress variable. The turbulent flame speed required for the reaction progress variable source term closure is calculated using the Peters' model [15]. Because convective heat transfer occurs along the combustor liner, the look-up tables are generated considering non-adiabatic conditions.

The GRI-Mech 3.0 reaction mechanism [20] was chosen to generate the table. This mechanism includes 53 chemical species and 325 reversible reactions, making it especially well-suited for fuels primarily composed of methane, along with other light hydrocarbons such as ethane and propane. Its use aligns well with the natural gas composition data provided by EthosEnergy. Since methane is the main component in the majority of the studied operating conditions, GRI-Mech 3.0 was selected over alternatives like the San Diego mechanism [21] and the CRECK Mechanism from Politecnico di Milano [22]. These alternatives are more appropriate for fuel blends with higher hydrogen content; in contrast, the San Diego mechanism is less suitable for heavier hydrocarbons, while the CRECK mechanism tends to be more computationally intensive. As the hydrogen content remains below 50% by volume, GRI-Mech 3.0 was adopted in line with recommended practices in the literature [23]. This mechanism, which features a range of NO_x formation pathways, is also used later in the CRN (Chemical Reactor Network) model for the NO_x emissions evaluation.

3.1 Boundary Conditions

The inlet boundary conditions are applied at the injector interface by using profiles (velocity, total temperature, mixture fraction) retrieved from the injector simulation as discussed in [14][15]. This approach allows for reduced computational costs and provides more flexibility in testing for redesigned configurations, since the reactive setup simulating the combustion chamber remains unchanged. Other boundary conditions consist of the outlet static pressure, air mass flow rate for the annulus region (green region in Figure 1) and dome cooling mass flow rate.

A synthesis of the applied boundary conditions is reported in Table 1.

Table 1: Boundary conditions.

Boundary Type	Boundary Condition
Air inflow (annulus) ■	Mass flow rate, total temperature, FGM variables ($c = 0$, $f = 0$)
Injector Inflow ■	velocity profiles, static temperature, FGM variables ($c = 0$, f - *profile*)
Combustor outlet ■	Static pressure

Regarding heat transfer in the liner, the convective heat transfer coefficient (h) values are specified alongside the solid material properties of the liner, which consists of a base material layer and a thermal barrier coating supplied by EthosEnergy. The *h* values vary between the two liners (420 and 250 W/(m2 K)), with the outer liner (the one at the larger radius) having

a higher coefficient due to the differing velocity fields present within the annulus.

The terminal section of the liner is cooled using full-coverage film cooling (FCFC) to maintain its durability against the harsh temperature conditions inside the combustion chamber. Cold air from the compressor is introduced into the combustor through several rows of small-diameter, inclined cylindrical channels located between the outer annulus and the liner. This method produces a thin protective layer of cool gas that isolates the liner from the hot combustion gases (see details in Figure 1). A uniform perforated wall boundary condition is applied to the upper and bottom sides of the liner to model the cooling, keeping the computational costs low. Further details regarding the model and the definition of the boundary conditions are widely discussed in [15].

3.2 NO_x Emissions

NOx emissions are a crucial factor in the operation of gas turbines, particularly in light of current regulatory standards. As extensively discussed in [15], when hydrogen is added at concentrations exceeding 30% by volume, the conventional decoupled method for calculating NO_x tends to underestimate the actual trend. In such cases, a CRN (chemical reactor network) model that incorporates the NNH pathway is necessary. [24].

As a result, a CRN model was employed using an ANSYS® tool [15] to account for additional formation pathways. Starting from a converged RANS simulation, the solver partitions the control volume into a series of Perfectly Stirred Reactors (PSRs), within which a detailed reaction mechanism is resolved. These reactors are connected by mass fluxes calculated from CFD results. The pressure used for chemical reaction calculations is assumed to match the average pressure of the corresponding CFD cells, while the temperature is determined using the equation of state, since the energy equation is not solved. Nevertheless, it is important to verify that the resulting temperature field is consistent with that from the RANS simulation. Clustering is based on grouping zones with uniform temperature or mixture fraction. The number of reactors ($N_{reactor}$) can be set by the user. Still, it should not be excessively high to retain physical relevance for each reactor (such as the main premixed flame, pilot diffusive flame, lateral recirculation region, or central recirculation zone). In this study, the number is set to 30, as a larger value would cause excessive subdivision and result in inaccurate temperature fields. The mass fractions (Y_k) for each reactor are computed using equation 1:

$$\sum_{j=1,j\neq i}^{N_{reactor}} \dot{m}_{ij} Y_k^j - \dot{m}_i Y_k^i = V_i \dot{\omega}_k^i + S_k^i \qquad (1)$$

where $\dot{m}$ represents the mass flow rate among the reactors, Y_k is the mass fraction the species k, $\dot{\omega}$ represents the species reaction rate and S is the mass source term. A set of equations is finally resolved for $N_{reactor} \times N_{species}$. The adopted chemical mechanism in this study is the GRI-Mech 3.0, the same used to generate the FGM tables.

4 H_2 Addition Effects

In this section, the effects of hydrogen addition in terms of flame shape, thermal stresses and NO_x emissions are recalled from [15] and used as guidelines for the injector redesign.

4.1 Thermal Effects and Injector Maintenance

To visualise the results from the CFD analysis, the domain is cut using two slices (see Figure 3), one in the longitudinal direction (indicated with the letter "a") and one in the transversal direction (indicated with the letter "b").

Figure 4 shows instead the temperature contours in the two main planes of the combustor. A high-temperature region is clearly visible in yellow, caused by the presence of the pilot flame. This flame is of a diffusive type and slightly deviates from the combustor centerline due to the presence of strong swirl, as can also be seen from the deviation of the premixed jets exiting the main (dark blue region). The temperature is almost uniform in the rest of the domain, while the quenching effect of the dilution holes is visible at the end of the domain.

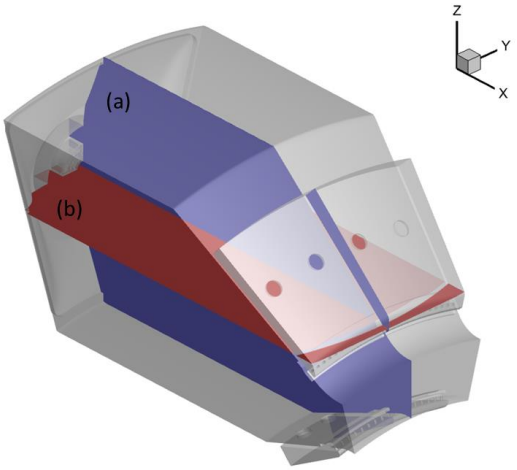

Figure 3: Section slices for the post-processing.

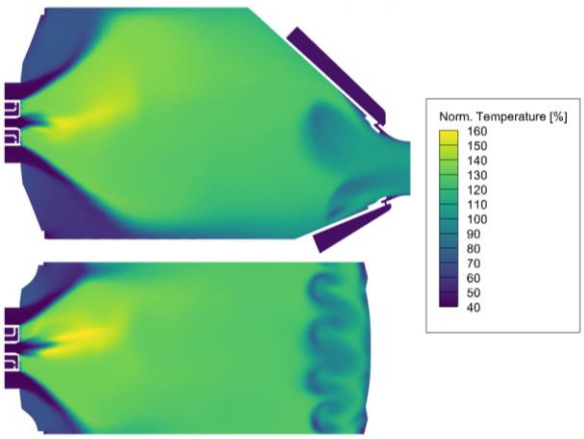

Figure 4: Temperature field contours in the two main planes of the combustor.

When examining the temperature maps, it is also possible to consider the OH contours shown in Figure 5. Areas with high OH concentrations align with the regions of elevated temperature, offering useful insight into the flame's position. The central core represents the pilot diffusive flame, which appears detached from the injector. Furthermore, a deviation of the pilot flame from the central axis can be observed, as previously noted. Another region of high reactivity is observed at the interface between the diffusive flame and the jets originating from the Main injector. This phenomenon can be attributed to a secondary flame, associated with the premixed portion of the mixture, which burns at a lower temperature. It is also evident that this zone - characterised by an OH mass fraction of 0.0006 and represented in green - is induced by the Pilot flame, as it is positioned at approximately the same axial location as the OH peak of the diffusive flame. This aligns with the role of the Pilot flame, which is to ensure flame stabilisation within the combustor under study.

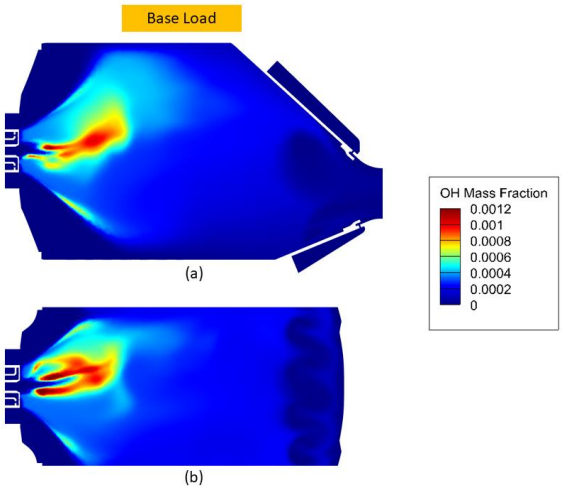

Figure 5: OH Mass Fraction in the two main planes of the combustor – Natural Gas.

The hydrogen addition consistently alters the flame shape by shortening the flame length as a result of the increased flame speed. These effects, widely discussed in the literature, can also be observed in the case under investigation. A detailed analysis of several blends is available in [15], while here the 50% in volume of H_2 case is discussed in more detail, since this is the case for which a consistent variation has been observed.

Figure 6 shows the OH plot for the 50% in volume case.

By comparing this case with the natural gas case, it is clear that the high-temperature region is larger with a potential increase in NO_x production. Furthermore, the peak temperature increases since the pilot flame is diffusive, and it is directly correlated to the LHV of the fuel blend. Finally, the flame becomes shorter and it is attached to the injector (as can be seen by comparing slices b from Figure 5 and Figure 6) with an increased risk of flashback and increased thermal stress.

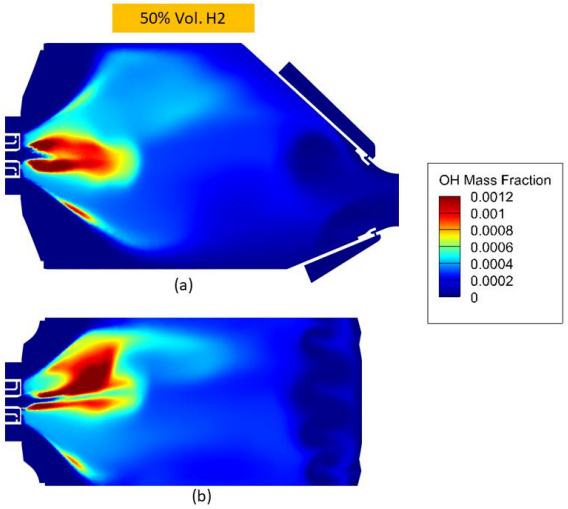

Figure 6: OH Mass Fraction in the two main planes of the combustor – 50% H_2 Vol.

The thermal stress is indeed a relevant issue for the machine under investigation. During the gas turbine overhaul, an unusual pattern was observed in the distribution of the thermal-stressed areas. The presence of a diffusive flame in the pilot region surely contributes to thermal stress on the combustor. To protect the injector from damage, effusion cooling is implemented in the head-end region. Nevertheless, periodic overhauls remain necessary. Since direct measurement of flame shape is often challenging in industrial gas turbines, it is helpful to correlate the degree of wear in operating plants with CFD simulation maps, as detailed in [15].

The analysis performed in [15] revealed a direct correlation between the high-temperature region generated by the diffusive flame of the Pilot and the areas exhibiting greater deterioration during inspections. The presence of hydrogen, producing a shorter flame, could exacerbate the thermal wear of the head-end region. Hence, it is clear that the use of hydrogen represents a challenge for the injector under investigation and it is necessary to adopt an alternative redesign to reduce the thermal stress on the head-end region and mitigate the risk of flashback.

4.2 NO_x Emissions Trends

In addition to the increase in thermal stress and flashback risk, the use of hydrogen also induces an increase in NO_x emissions. The reasons behind this increase can be related to multiple factors, such as the increase in the peak temperature and the presence of hydrogen-induced formation pathways [24].

As a result, as shown in [15], traditional post-processing approaches are inadequate to predict the NO_x emissions, and for these reasons, a CRN approach is here adopted as discussed in section 3.2.

The NO_x emissions expressed in *ppmvd* at 15% O_2 are reported in Figure 7.

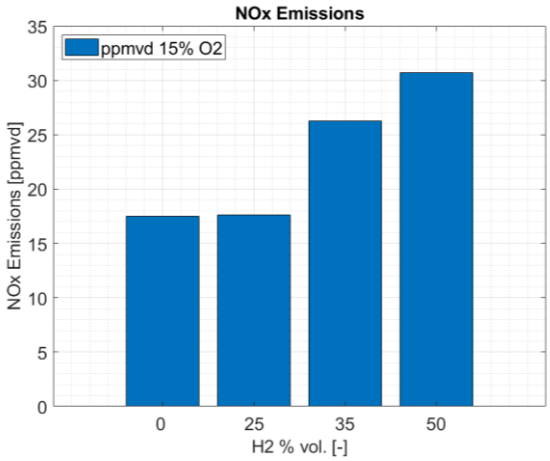

Figure 7: NO_x Emissions – base design.

The emission trend remains stable up to 25% of hydrogen in volume, while it shows a sharp increase starting from 35%, with its value almost doubled at 50%. These results lead to a further need for the injector redesign to keep the NO_x emissions constant when different fuel blends are used in operations.

The data acquired from the CFD analysis with hydrogen blends used with the standard injector design have been used as a basis for the redesign concept shown in Section 5, together with some indications regarding flame stabilisation available in literature.

The concept will then be numerically tested in Section 6.

5 Redesign Strategy

In this section, the redesign strategy is shown, starting from the information retrieved from the CFD simulations and considering a set of requirements in terms of emissions, thermal wear and flame stabilisation.

The redesign guidelines applied to the Pilot circuit considered in this work are the following:

- flame stabilisation for both natural gas and hydrogen blends;
- modular design allowing for fuel composition switch;
- flame shape similar to the design case with no increase of thermal load on the injector;
- constant NO_x emissions equal to the natural gas conditions;
- combustion oscillations suppression.

From the previous analysis, it is clear that the Pilot is the main component that needs to be redesigned and in particular, two main objectives need to be achieved:

1. increase in the injection velocity to move the flame forward;
2. reduce the flame temperature of the Pilot flame, which is diffusive.

The main characteristics of the injector are summarized in Table 2; notice that the equivalence ratio of the Pilot is rich.

Table 2: Injection Condition – Design Natural Gas.

Equivalence Ratio - Main	0.55
Equivalence Ratio - Pilot	1.192
Pilot Jet Velocity	55 m/s

A possible solution consists of increasing the mass flow rate of air through the Pilot, hence increasing the injection velocity and changing the equivalence ratio of the Pilot flame at the same time. The redesign concept is shown in Figure 8.

The redesigned version presents an additional channel that allows for an increased air mass flow rate. The air path is also changed when switching to the new configuration: in the standard one, the air flowing through the annular channel is partially directed to the cooling of the head-end region, while the rest is mixed with the fuel in a counter-flow configuration. In the redesigned version, the air flows in the same direction as the fuel and the overall air mass flow rate is increased, not only the air premixed with the fuel, but also the air used to cool down the injector front plate.

The central region of the injector, where the mixing between air and fuel occurs tog ether with the creation of a swirling motion, is not shown due to confidentiality reasons. In any case, this region is not subjected to any change in the redesign phase, so the detailed mechanism of mixing is beyond the scope of this work.

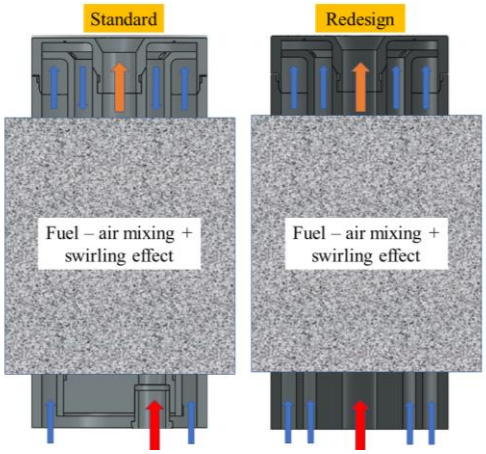

Figure 8: Pilot Redesign Concept.

The new design should also guarantee constant performance with natural gas: this goal is achieved by using a blocking ring that prevents air from flowing in the new additional annular channel. In this configuration, the air flows again in counterflow with respect to the fuel as in the standard design. The use of the blocking ring is shown in Figure 9. This blocking ring can be mounted on the injector during the overhaul phase, since the specific customer can specify the fuel composition that will be used with the machine.

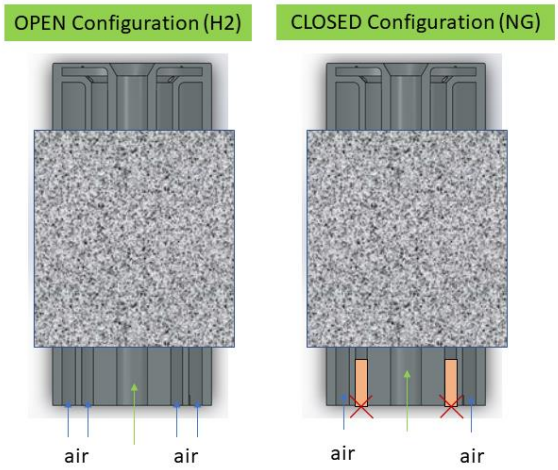

Figure 9: Use of a blocking ring for NG operations.

A useful tool during the redesign phase is to evaluate the effects of the different geometries in terms of equivalence ratio at the chemical equilibrium in order to estimate the temperature at the outlet of the combustor and in the Pilot flame. A parametric study using the chemical equilibrium reactor in ANSYS® Chemkin® 2022 R2 has been used to compute the adiabatic flame temperature curves at relevant equivalence ratio ranges for both natural gas and 50% of hydrogen by volume blends. The chemical mechanism is the same used for the FGM table generation and the CRN computations, the GRI-Mech 3.0. The blend compositions are reported in Table 3, namely the same adopted in [15] and obtained starting from the natural gas composition and uniformly rescaled to accommodate the presence of hydrogen.

Table 3: Fuel blend compositions.

Species	Volume Fractions		
H_2	0.000		0.500
CH_4	0.865		0.432
CO_2	0.033		0.016
C_2H_6	0.065		0.032
N_2	0.007		0.003
C_3H_8	0.031		0.016

The resulting Adiabatic Flame Temperature (AFT) curves obtained at relevant gas turbine conditions (inlet temperature equal to the compressor discharge temperature and operating pressure equal to the turbine inlet pressure) are reported in Figure 10 in normalised form with respect of the outlet combustor temperature in Base Load conditions, for equivalence ratios between 0.3 (overall equivalence ratio) and 1.3 (Pilot rich conditions).

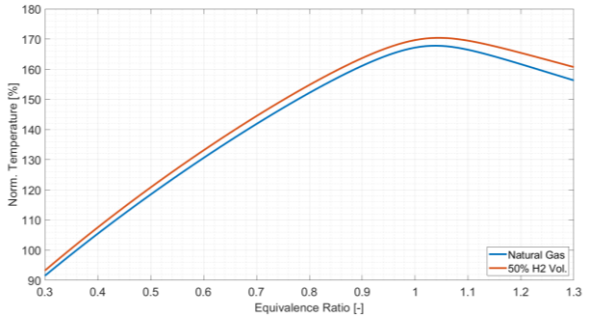

Figure 10: Adiabatic Flame Temperature for different Equivalence Ratios.

To understand the idea behind the Pilot redesign, let's focus the analysis on the equivalence ratio range relevant for the Pilot. A zoom of the AFT curves in the range 0.7 – 1.2 is reported in Figure 11.

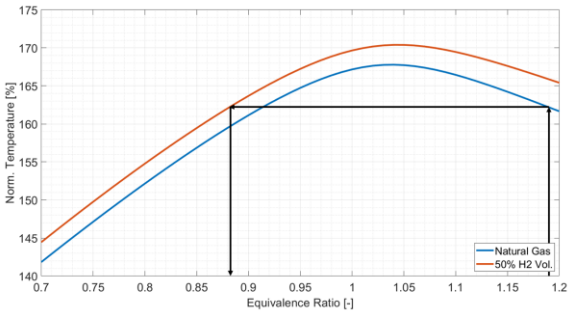

Figure 11: Adiabatic Flame Temperature (AFT) for Equivalence Ratio in the range [0.7 – 1.2] – ER estimation for the Pilot.

The main idea behind the redesign is to identify the equivalence ratio (ER) value for the 50% hydrogen blend in the lean region that presents the same AFT as the natural gas case (Pilot ER equal to 1.19). This value corresponds to an ER of 0.88, thus guaranteeing a similar flame temperature for the Pilot together with an increased injection velocity thanks to the increased air mass flow rate.

At this point, a verification of the overall ER is needed to guarantee a constant turbine inlet temperature (TIT). The results in terms of equilibrium temperature are reported in Figure 12, where a detailed plot of the AFT in the lean regime is shown.

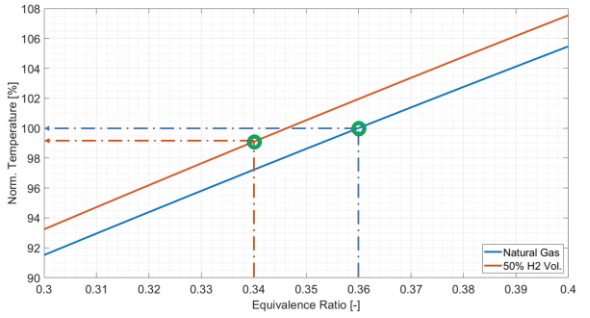

Figure 12: Adiabatic Flame Temperature (AFT) for Equivalence Ratio in the range [0.3 – 0.4] – Turbine Inlet Temperature (TIT).

The use of the redesigned injector leads to a global ER of 0.34 against a value of ER equal to 0.36 for the natural gas case. The difference in terms of temperature is below 1% (less than 10 K) and will not affect the turbine performance. However, a cold flow test performed on the proposed redesigned Pilot, following the procedure reported in [14], reports a value of ER value equal to 0.7, potentially too low to guarantee safe operations and flame stabilisation since the Pilot flame temperature will be lower than the design value, thus implying a possible risk of flame extinction and combustion instability.

To limit the air mass flow rate, it is needed to reduce either the inlet cross-section by limiting the area in the new annular section or by limiting the inlet total pressure. The first method would be most natural; however, it was not possible to achieve the target mass flow rate by reducing the inlet cross-section.

The ER as a function of the inlet cross-section is shown in Figure 13. To achieve the target ER of around 0.88 or higher, the inlet area should be considerably small, resulting in a gap below 0.3 mm.

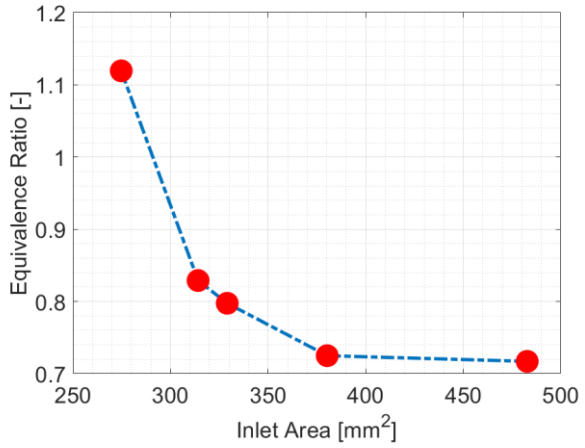

Figure 13: ER vs Inlet Area, constant fuel flow rate.

Since the reduction of the inlet cross-section is not practically achievable for this geometry, a different strategy needs to be adopted for this test case.

A possible alternative, adopted in this work, is to adjust the inlet total pressure of air by introducing an additional concentrated pressure loss upstream of the Pilot inlet, thus reducing the inlet total pressure and hence the air mass flow rate.

The geometry shown in Figure 8 is therefore studied under cold flow conditions for several inlet air total pressures, with the fuel flow rate kept constant; the results are presented in Figure 14.

The selected operating point is the one with an equivalence ratio of 0.93. This value helps in minimising the gap with the nominal TIT (see Figure 12), while ensuring enhanced stability for the flame, thanks to the presence of hydrogen addition that extends the operational limits, reducing the risk of lean blow-off (LBO) [25].

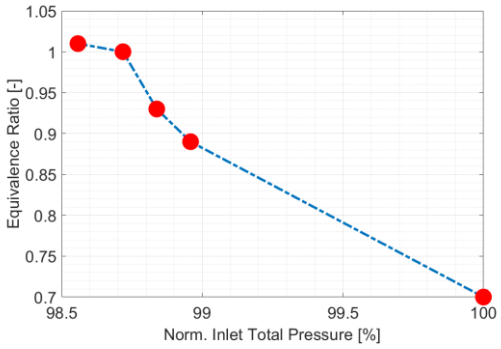

Figure 14: ER vs Inlet Total Pressure, constant fuel flow rate.

Li et al. [26] showed, through a coupled experimental and numerical approach, that for a swirled-stabilised combustor with a central pilot, the amplitude of instability is largely unaffected by changes in the pilot mass flow rate once a small flow rate threshold is passed, but it is highly influenced by the pilot's equivalence ratio. Specifically, the effectiveness of the pilot increases as its equivalence ratio gets closer to that of the main flame; beyond this point, further increases in the pilot's equivalence ratio have a less pronounced effect on thermo-acoustic instability. From these observations, the authors proposed that a central pilot flame helps mitigate thermoacoustic instability by supplying heat and radical species to the base of the main flame, facilitated by recirculation within the vortex breakdown bubble. This back-support stabilises the main flame both statically and dynamically. These results also suggested that a low pilot flow rate of a mixture slightly richer than the main flame can significantly enhance pilot effectiveness without causing a notable increase in NO_x emissions [26].

These findings are applied here to an industrial case, showing the feasibility of this kind of redesign for NO_x abatement in contrast to traditional designs with rich pilot, developed in a period where the numerical methods were less reliable than nowadays and the literature on experimental data on pilot flames was limited. In particular, the pilot equivalence ratio is still higher than the main equivalence ratio, without reaching rich conditions, and at the same time, the jet velocity will increase, thus moving the flame downstream. The results of the reactive CFD analysis are reported in the next subsection.

6 Results

In this section, the redesigned concept is tested at 50% volume of hydrogen to analyze its behavior in terms of temperature distribution, emissions, and stability, to understand whether the hypothesis adopted for the redesign is valid.

The first element to be verified is the injection velocity for the Pilot jet. The mass flow rate of air has been increased through the redesign process, which should result in a higher velocity value. The velocity contour for the primary zone is reported in Figure 15.

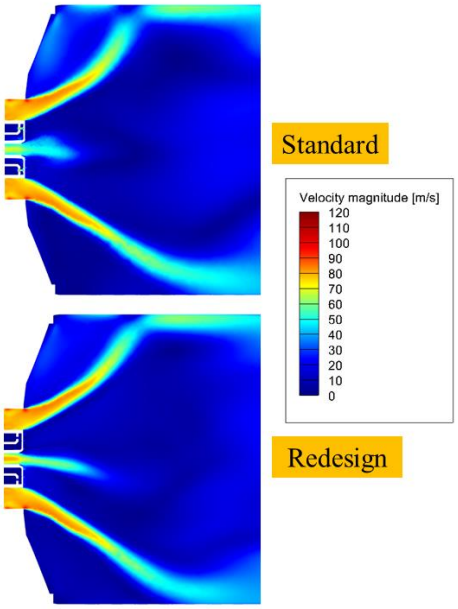

Figure 15: Velocity Magnitude, Standard Vs Redesign configurations at 50% H_2 in Vol.

By comparing the velocity maps for the standard and redesigned cases, the velocity of the Pilot Jet is higher in the redesigned configuration. The original mean jet velocity of approximately 55 m/s is increased to 70 m/s here, thereby reducing the risk of flashback in the event of hydrogen addition. Additionally, because of the increased injection velocity, the jet penetration is also increased, and this will allow for flame stabilization away from the injector.

To verify the change in flame shape, position, and temperature distribution, the OH contour is reported in Figure 16.

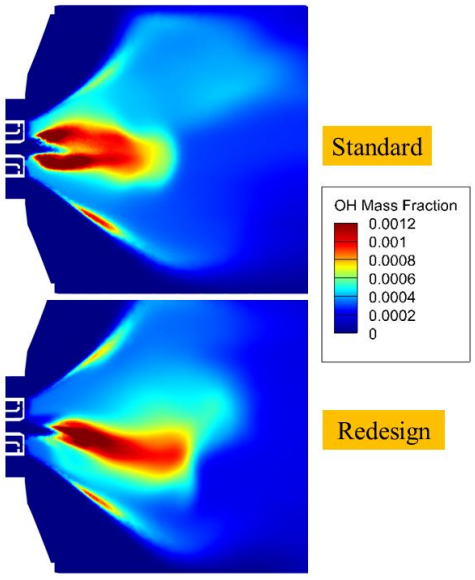

Figure 16: OH Mass Fraction, Standard Vs Redesign configurations at 50% H_2 in Vol.

In the original injector, the flame is attached to the head-end plate for the fuel blend with 50% of hydrogen. The resulting thermal stress would be too high, thus reducing the typical life span. For the redesigned version, instead, the flame appears to be detached and far away from the injector and hence the thermal stress results in being reduced. It is also interesting to notice how the flame is even more downstream if compared to the standard design with natural gas, meaning that the redesign is beneficial for the lifetime of the injector.

Another interesting feature for the flame stability is the position of the Main flame. The location of the Main flame can be identified by looking at the OH peak present at the interface between the Main jet and the inner recirculation zone. The OH distribution is indeed the same, meaning that the flame is stabilised at the same average position by the Pilot, thus excluding any considerable change in the overall flame shape, also for the Main.

An additional check is related to the surface temperature profile of the injector, as shown in Figure 17. The use of hydrogen with the standard configuration induces an increased thermal stress since the flame is attached to the injector. The redesigned configuration shows instead a reduced thermal load and a detached flame.

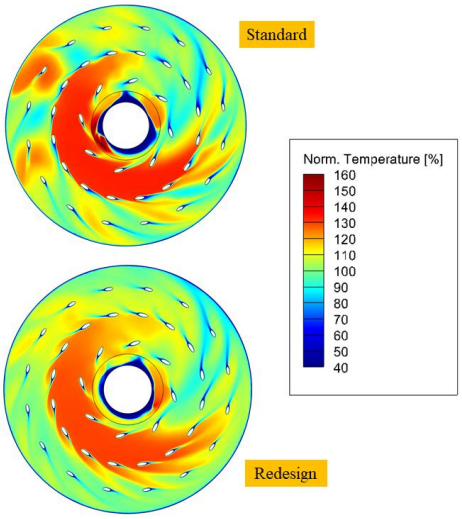

Figure 17: Normalised Surface Temperature Maps, Standard Vs Redesign at 50% H_2 in Vol.

Finally, the NO_x emissions levels are compared in Figure 18, showing the emissions expressed in *ppmvd* at 15% of O_2 for the natural gas case, the blend with 50% in volume of hydrogen and the same blend with the redesigned Pilot.

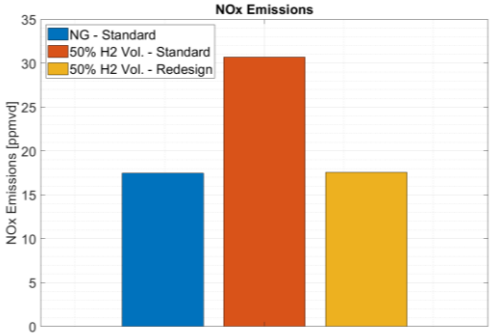

Figure 18: NO_x Emissions, Base Design Vs Redesign.

The emissions levels for the redesigned injector are comparable to the natural gas values and equal to 17.5 *ppmvd*, thus ensuring constant emissions also when hydrogen is used in the fuel blend, drastically reducing the value obtained without redesign, equal to 30.7 *ppmvd*.

7 Conclusion

The present work explores a possible redesign approach for the injector of a DLN combustor for hydrogen applications. In particular, reactive CFD simulations are employed to assess the impact of hydrogen addition up to 50% by volume in the fuel blend. The results indicate increased thermal stress on the injector, along with higher NO_x emissions. This trend is mainly attributed to the presence of a diffusive Pilot flame, which is necessary for flame stabilization. Building on recent experimental studies on instability suppression mechanisms associated with the Pilot flame, the injector is redesigned by adjusting the operating point in terms of equivalence ratio. This approach preserves the mechanical integrity of the injector while ensuring reduced NO_x emissions, thereby demonstrating the feasibility of such a redesign strategy for similar machines, enabling the use of hydrogen blends with only minor modifications.

Acknowledgements

We acknowledge the CINECA award under the ISCRA initiative for the availability of high-performance computing resources and support within the ISCRA-C project SISSI. HPC@POLITO also provided computational resources.

References

[1] Lewis G. D. Prediction of NOx Emissions. ASME Gas Turbine Conference & Products Show, March 9-12, 1981, Houston, Texas. 81-GT-119

[2] Energy Technology Perspectives 2020; International Energy Agency: Paris, France, 2020.

[3] Campbell, A.; Goldmeer, J.; Healy, T.; Washam, R.; Molière, M.; Citeno, J. Heavy Duty Gas Turbines Fuel Flexibility. In Proceedings of the Turbo Expo: Power for Land, Sea, and Air, Berlin, Germany, 9–13 June 2008; pp. 1077–1085.

[4] Shelil, N, Griffiths, A, Bagdanavicius, A, & Syred, N. "Flashback Limits of Premixed H2/CH4 Flames in a Swirl-Stabilized Combustor." Proceedings of the ASME Turbo Expo 2010: Power for Land, Sea, and Air. Volume 2: Combustion, Fuels and Emissions, Parts A and B. Glasgow, UK. June 14–18, 2010. pp. 1247-1258. ASME.

[5] Noble, D.; Wu, D.; Emerson, B.; Sheppard, S.; Lieuwen, T.; and Angello, L. Assessment of Current Capabilities and Near-Term Availability of Hydrogen-Fired Gas Turbines Considering a Low-Carbon Future. Journal of Engineering for Gas Turbines.

[6] Hydrogen Gas Turbines Report 2024 Edition, ETN Global Report

[7] Pennell, D, Tay-Wo-Chong, L, Smith, R, Sierra Sanchez, P, & Ciani, A. "GT36 First Stage Development Enabling Load and Fuel (H2) Flexibility with Low Emissions." Proceedings of the ASME Turbo Expo 2023: Turbomachinery Technical Conference and Exposition. Volume 3B: Combustion, Fuels, and Emissions. Boston, Massachusetts, USA. June 26–30, 2023. V03BT04A045. ASME.

[8] zur Nedden, P.M.; Eck, M.E.G.; Lückoff, F.; Panek, L.; Orchini, A.; Paschereit, C.O. Flame Transfer Function and Emissions of a Piloted Single Jet Burner: Influence of Hydrogen Content. Proceedings of the ASME Turbo Expo 2023: Turbomachinery Technical Conference and Exposition. Volume 3B: Combustion, Fuels, and Emissions. Boston, Massachusetts, USA. June 26–30, 2023. V03BT04A017

[9] Petry, N., Mannazhi, M., Yin, Z., Lammel, O., Geigle, K. P., and Huber, A. (December 26, 2023). "Investigation of Fuel and Load Flexibility of an Atmospheric Single Nozzle Jet-Stabilized FLOX® Combustor With Hydrogen/Methane-Air Mixtures." ASME. J. Eng. Gas Turbines Power. June 2024; 146(6): 061004.

[10] Hohloch, M, Lingstädt, T, & Kutne, P. "Experimental Analysis of the Hydrogen Capability of a Fuel Flexible Jet Stabilized Syngas Micro Gas Turbine Combustor Under Atmospheric Conditions." Proceedings of the ASME Turbo Expo 2023: Turbomachinery Technical Conference and Exposition. Volume 3B: Combustion, Fuels, and Emissions. Boston, Massachusetts, USA. June 26–30, 2023. V03BT04A039.

[11] Carusotto S., Goel P., Baratta M., Misul D.A., Salvadori S., Cardile F., Forno L., Toppino M., Valsania M., 2022. Combustion Characterization in a Diffusive Gas Turbine Burner for Hydrogen-Compliant Applications. MDPI Energies, Special Issue “Advances and Advantages in CFD Analysis of Gas Turbine Combustors”, Vol 15, Issue 11, No. 4117 (20 pages), doi: 10.3390/en15114117.

[12] Carusotto, S., Labrini, G., Salvadori, S., Baratta, M., Cardile, F., Toppino, M., Valsania, M., and Misul, D. (October 26, 2023). "Evaluation of Nox Emissions Associated to Non-Premixed Combustion of H2/Natural Gas Blends in a 40 MW Heavy-Duty Gas Turbine." ASME. J. Eng. Gas Turbines Power. December 2023; 145(12): 121020.

[13] Köhler, M, Hiestermann, M, & Müller, H. "Numerical Investigation of Steam Injection in a Premixed Swirl-Stabilized Methane-Air Flame Using the Flamelet-Generated-Manifold Method." Proceedings of the ASME Turbo Expo 2023: Turbomachinery Technical Conference and Exposition. Volume 3B: Combustion, Fuels, and Emissions. Boston, Massachusetts, USA. June 26–30, 2023. V03BT04A037. ASME.

[14] Carusotto S., Salvadori, S., Cavalli A., Casto E., Cardile F., Misul D.A., 2024. Characterization Of a Premixed Gas Turbine Injector for Light-Duty and Low Emissions Applications. Proc. of the ASME Turbo Expo 2024, London, UK, June 24–28, 2024, Volume 3B: Combustion, Fuels, and Emissions, ISBN 978-0-7918-

8795-0, doi: 10.1115/GT2024-129169, Paper No. GT2024-129169, V03BT04A069.
[15] Carusotto, S., Capalbo, N., Salvadori, S., Cavalli, A., Cardile, F., and Misul, D. (August 23, 2025). "Combustion Characterization Of An Industrial Gas Turbine Combustor For Low Emissions Applications Fed With Natural Gas/Hydrogen Blends." ASME. J. Eng. Gas Turbines Power.
[16] Ansys Fluent Theory Guide, Release 2022 R2. 2022.
[17] Yakhot, V.; Orszag, S.A.; Thangam, S.; Gatski, T.B.; Speziale, C.G. Development of turbulence models for shear flows by a double expansion technique. Phys. Fluids A Fluid Dyn. 1992, 4, 1510–1520.
[18] Patil, S.; Abraham, S.; Tafti, D.; Ekkad, S.; Kim, Y.; Dutta, P.; Moon, H.K.; Srinivasan, R. Experimental and Numerical Investigation of Convective Heat Transfer in a Gas Turbine Can Combustor. ASME J. Turbomach. 2011, 133, 011028.
[19] Van Oijen, J.A.; de Goey, L.P.H. Modelling of premixed laminar flames using Flamelet-Generated Manifolds. Combust. Sci. Technol. 2000, 161, 113–137.
[20] GRI-Mech 3.0 Gregory P. Smith, David M. Golden Michael Frenklach, Nigel W. Moriarty, Boris Eiteneer, Mikhail Goldenberg, C. Thomas Bowman, Ronald K. Hanson, Soonho Song, William C. Gardiner, Jr., Vitali V. Lissianski, and Zhiwei Qin (http://www.me.berkeley.edu/gri_mech/)
[21] San Diego reaction mechanism (https://web.eng.ucsd.edu/mae/groups/combustion/mechanism.html - accessed on 11/12/2024)
[22] CRECK Model – Politecnico di Milano (https://www.creckmodeling.polimi.it/menu-kinetics/menu-kinetics-detailed-mechanisms/)
[23] Zhao, R, Igie, U, Abbott, D, & Wiranegara, RY. "Co-Firing of Hydrogen and Natural Gas in a Practical DLN Combustor Model." Proceedings of the ASME Turbo Expo 2023: Turbomachinery Technical Conference and Exposition. Volume 3B: Combustion, Fuels, and Emissions. Boston, Massachusetts, USA. June 26–30, 2023. V03BT04A031. ASME.
[24] Purohit, A.L., Nalbandyan, A., Malte, P.C., Novosselov I.V. NNH mechanism in low-NOx hydrogen combustion: Experimental and numerical analysis of formation pathway. Fuel 292 (2021) 120186
[25] F. Pignatelli, D. Sanned, S. Derafshzan, R.Z. Szasz, X.S. Bai, M. Richter, A. Ehn, D. Lörstad, P. Petersson, A.A. Subash, Impact of pilot flame and hydrogen enrichment on turbulent methane/hydrogen/air swirling premixed flames in a model gas turbine combustor, Experimental Thermal and Fluid Science, Volume 152, 2024, 111124, ISSN 0894-1777
[26] Li, J., Kwon, H., Seksinsky, D., Doleiden, D., O'Connor, J., Xuan, Y., Akiki, M., and Blust, J. (October 18, 2021). "Describing the Mechanism of Instability Suppression Using a Central Pilot Flame With Coupled Experiments and Simulations." ASME. J. Eng. Gas Turbines Power. January 2022; 144(1): 011015.